Journal Name

ARTICLE

# Structure and Magnetic Properties of the $AB(HCO_2)_3$ (A = $Rb^+$ or $Cs^+$, B = $Mn^{2+}$, $Co^{2+}$ or $Ni^{2+}$) Frameworks: Probing the Effect of Size on the Phase Evolution of the Ternary Formates

Sally M. Bovill,[a] and Paul J. Saines[a,b*]

This work reports the synthesis and structures of six new $AB(HCO_2)_3$ (A = $Rb^+$ or $Cs^+$ and B = $Mn^{2+}$, $Co^{2+}$ or $Ni^{2+}$) frameworks containing the largest monoatomic cations on the A-site. $RbMn(HCO_2)_3$ is found to adopt a distorted perovskite framework with a $4^{12}\bullet6^3$ topology and a mixture of *syn-anti* and *anti-anti* ligands, while the remaining compounds adopt a chiral hexagonal structure with a $4^9\bullet6^6$ topology. The structures of these frameworks clarifies the effect of ionic size on the formation of the five known architectures adopted by the $AB(HCO_2)_3$ frameworks, which have attracted attention as a new class of potential multiferroics, and in particular the chiral hexagonal structure within this. This also highlights the role of molecular A-site cations in stabilising the $4^9\bullet6^6$ topology for frameworks where such cations are too large or small to support this structure on the basis of size alone, possibly due to hydrogen bonding. The magnetic properties of the $RbB(HCO_2)_3$ and $CsMn(HCO_2)_3$ frameworks are also reported with the $Rb^+$ compounds featuring weak ferromagnetic behaviour and the latter being purely antiferromagnetic. In conjuction with a comparison of the other isostructural $AB(HCO_2)_3$ frameworks we find that compounds adopting the $4^9\bullet6^6$ topology have much higher magnetic ordering temperatures than those with the $RbMn(HCO_2)_3$ structure, highlighting the importance of understanding the structure-property relationships of the ternary formates.

## 1. Introduction

Coordination frameworks, including dense Metal-Organic Frameworks (MOFs), have attracted significant attention in recent years for their ability to exhibit unique variations on the functional properties traditionally associated with metal oxides including magnetic order, multiferroicity, semi-conductivity and ionic conductivity.[1,2-4] This is due to the varied architectures they adopt because of the structure directing effect of the ligand, even while smaller ligands bring metal centres closer together enabling electronic communication between them. Magnetoelectrical properties include hydrogen-bond driven relaxor ferroelectric order,[5,6] guest-dependent magnetism[2,7] and new routes to multiferroic materials.[3,6,8] Arguably the most intriguing of these compounds are the $AB(HCO_2)_3$ frameworks, where A is a monovalent alkali metal, ammonium, imidazolium or a protonated alkylamine and B is typically a divalent first row transition metal.[4,6,9,10] Molecular A-site cations in these frameworks tend to exhibit hydrogen-bond driven order-disorder transitions, near to or below room temperature, often leading to the emergence of ferroelectric order.[5,6,11] They typically exhibit weak ferromagnetic order, arising from spin canting and, while the coupling of electric and magnetic order are very weak, the combination of these two facets in a framework leads to a new route to potential multiferroics.[3,4,12]

The $AB(HCO_2)_3$ frameworks with three dimensional covalent connectivity all feature octahedral B-site cations linked in a corner-sharing fashion through the formate ligand, with the A-site cation typically sitting in pockets found in the structure. Beyond that they can vary significantly with five different structure-types known, which can largely be classified by their topologies and the coordination modes the formate ligands bind in (see Fig. 1).[11] Those compounds accommodating the largest A-site cations, usually moderately sized alkylamines, such as $(CH_3)_2NH_2$, or imidazolium, adopt a perovskite-like structure with a $4^{12}\bullet6^3$ topology.[11,13] Herein this structure is referred to as Perovskite I, consistent with Gómez-Aguirre *et al.*[11], and has all ligands binding the B-site metals in an *anti-anti* fashion. Two other $4^{12}\bullet6^3$ topologies have been discovered for the $AB(HCO_2)_3$ frameworks. The first, so-called Perovskite II, is the thermodynamically preferred phase where the A-site cation is $K^+$ and the B-site cation is $Mn^{2+}$, $Co^{2+}$ and $Cd^{2+}$;[10,14,15] each B-site cation is connected to six others via a mixture of *syn-anti* and *anti-anti* ligands. In this structure every second channel down the *c*-axis is occupied by A-site cations while the formate hydrogen atoms fill the other. Perovskite III is adopted by $NH_4Cd(HCO_2)_3$,[11] which is polar at ambient temperature, and a less common polymorph of $NH_4Mn(HCO_2)_3$.[8] This structure closely resembles Perovksite II except all ligands connect $M^{2+}$ in a *syn-anti* arrangement.

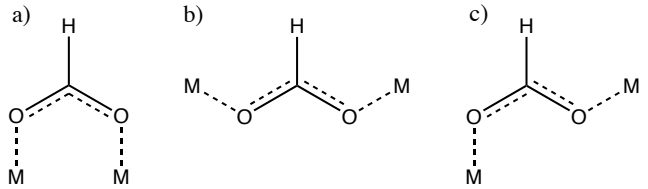

**Fig. 1:** Possible different coordination modes of the formate anion: a) *syn-syn*, b) *anti-anti* and c) *syn-anti*.

Two structures with other topologies have currently been observed in the $AB(HCO_2)_3$ family. Those containing smaller $Na^+$ A-site cations adopt a chiral cubic structure with a $3^3•5^6$ topology and all linkers adopting a *syn-anti* arrangement.[10,16,17] Chiral hexagonal or pseudo-hexagonal phases with a $4^9•6^6$ topology are also known to form where the A-site cation is a small molecule such as $NH_4^+$,[6,18] $HONH_3^+$,[19] or $NH_2NH_3^+$ (the later only when B is $Co^{2+}$ and $Mg^{2+}$)[5]. In this architecture all linkers adopt an *anti-anti* configuration. The $NH_4^+$ members are known to adopt a polar structure at low temperature with ferroelectric or relaxor-like ferroelectric properties[6] while the properties of the $NH_2NH_3^+$ compounds are also fascinating as, unusually, they undergo a transition from an antiferroelectric phase to polar phases as a result of partial cation disordering.[5]

The relative sizes of the cations plays a critical role in determining which of these five structures are adopted by the $AB(HCO_2)_3$ frameworks. Kielslich *et al*.[20] have recently defined a tolerance factor for hybrid phases extending the classic concept of tolerance factors, traditionally used to judge whether the relative sizes of cations and anions in an $ABX_3$ ionic solid will lead to a perovskite phase, to those containing molecular building blocks. Their formularism is $\alpha = \left(r_{A,eff} + r_{x,eff}\right)/\sqrt{2}\left(r_B + 0.5h_{x,eff}\right)$, where *r* refers to the effective molecular or ionic radius of the A-site, B-site and X(anionic)-site while $h_{x,eff}$ refers to the height of the anions in the direction between B-site cations. According to this almost all the $AB(HCO_2)_3$ compounds with an $\alpha$ of between 0.80 and 1 adopt the Perovskite I phase as expected from their ionic counterparts.[13,20] Gómez-Aguirre *et al*.[11] have recently extended the use of the tolerance factor to rationalize the order in which other $AB(HCO_2)_3$ phases appear. They find that Perovskite II is stable for an intermediate tolerance factor range, approximately $0.64 < \alpha < 0.69$, and that $NH_4Cd(HCO_2)_3$, the only compound for which Perovoskite III has been isolated as a pure phase, has an $\alpha$ of 0.63.[i] The inclusion of $Na^+$ decreases the tolerance factor further, to below 0.60 leading to the adoption of the chiral cubic phase. They were, however, unable to explain the adoption of the $4^9•6^6$ chiral hexagonal structure in this scheme, which they described as spanning a range of $0.65 < \alpha < 0.68$ citing the $NH_4B(HCO_2)_3$ series, which overlaps with the Perovskite II series range.[11] Indeed the situation is even more complex than this as chiral hexagonal structures containing $HONH_3^+$ and $NH_2NH_3^+$ cations have tolerance factors as high as 0.85, well into the range of the Perovskite I structure.[13,19,21] Clearly other factors beyond ionic radii will influence the structures adopted by some of these materials e.g. the specific shape of the molecular guest and the precise hydrogen bonds it forms with frameworks may favour some structure types over others. It is also likely that polymorphism is present in some of these cases, found for $NH_4Mn(HCO_2)_3$[8,18] and $KCo(HCO_2)_3$,[14] where in the later the kinetic product adopts a chiral hexagonal phase. Given the versatility and ease of use of the tolerance factor, however, it is clearly valuable for giving an approximate indication of what structure is likely to form in the fascinating $AB(HCO_2)_3$ family, particularly in the cases where size effects are primarily responsible for the phases adopted. In an attempt to do this, and in particular clarify the position of the $4^9•6^6$ chiral hexagonal structure in this hierarchy, we have synthesised the $AB(HCO_2)_3$ frameworks where A = $Rb^+$ or $Cs^+$ and B = $Mn^{2+}$, $Co^{2+}$ or $Ni^{2+}$. These compounds contain the largest possible monoatomic A-site cations, which leads to higher tolerance factors in the range of 0.66 to 0.73. Here we report the structure of these materials, clarifying the effect of size on the sequence of phases adopted by the $AB(HCO_2)_3$ family, along with their magnetic properties and thermal stability.

## 2. Experimental

The compounds synthesized in this work were obtained using a method similar to Eikeland *et al*.[10] using commercially available reagents. In a typical synthesis 10 mL of 0.73 M $HCO_2H$ (reagent grade 95 %, Sigma-Aldrich) and 0.2 M of either $RbOH•xH_2O$ or $CsOH•H_2O$ (Sigma-Aldrich) in anhydrous methanol (Sigma-Aldrich 99.8 %) was placed at the bottom of a glass tube. 10 mL of 0.025 M of $MnCl_2•4H_2O$ (99+ % Across Organics), $CoCl_2$ (97 %, Sigma Aldrich) or $NiCl_2•6H_2O$ (99.3 % Alfa Aesar) in anhydrous methanol was carefully layered on top. The tube was then sealed and kept undisturbed for up to two weeks, until crystals formed. This led to single crystals of $RbMn(HCO_2)_3$, $CsMn(HCO_2)_3$, $RbNi(HCO_2)_3$, $CsNi(HCO_2)_3$ and $RbCo(HCO_2)_3$ suitable for structure determination, the first three of these in pure form. A pure sample of $RbCo(HCO_2)_3$ was made using two 10 mL methanol solutions of 1.46 M $HCO_2H$ and 0.6 M $RbOH•xH_2O$, and 0.05 M $CoCl_2$. Single crystals of $CsCo(HCO_2)_3$ suitable for structural determination were obtained by decreasing the bottom layer concentrations to 0.365 M $HCO_2H$ and 0.1 M $CsOH•H_2O$.

Single crystal structure determinations were carried using two diffractometers, a Nonius Kappa CCD equipped with Mo K$\alpha$ radiation, generated by a conventional generator operating at 60 kV and 30 mA, and a dual source Oxford Diffraction Supernova equipped with Mo K$\alpha$ and Cu K$\alpha$ micro-focus sources, operating at 0.8 kV and 50 mA, with multilayered focusing optics and a Atlas CCD detector (see Table 1 for crystallographic details). Samples were cooled to 150 K using a Oxford Cryosystem cryostream with the samples held on a MiTeGen micro loop. Data were integrated and empirical or, in the case of $CsCo(HCO_2)_3$, analytical, absorption corrections performed using the DENZO/SCALEPACK suite[22] and the CrysAlisPro software suite version 171.36.32,[23] for the Nonius and Oxford Diffraction instruments, respectively. Structures were solved using direct or Patterson methods in SHELXS-2014[24] or charge-flipping in olex2.solve[25] and least-squares refinements were carried out using SHELXL-2014,[26] via the Olex2 graphical user interface.[27] The displacement parameters of non-hydrogen atoms were refined anisotropically and hydrogen atoms were typically located geometrically using the AFIX commands in SHELXL-2014,[26] with their displacement parameters constrained to 1.2 times that of the carbon on

which they rode. The crystal of $CsMn(HCO_2)_3$ used was a merohedral racemic twin with two equal components within the precision of the refinement.

**Table 1**: Crystallographic Data for structures **1**-**6** determined by single crystal X-ray diffraction. Structure **3** was determined using Cu Kα while Mo Kα radiation was used in all other cases.

| Compound | **1** | **2** | **3** | **4** | **5** | **6** |
|---|---|---|---|---|---|---|
| Formula | RbMnC3H3O6 | RbCoC3H3O6 | RbNiC3H3O6 | CsMnC3H3O6 | CsCoC3H3O6 | CsNiC3H3O6 |
| Formula Weight | 275.46 | 279.45 | 279.23 | 322.90 | 326.89 | 326.67 |
| T (K) | 150(2) | 150(2) | 150(2) | 150(2) | 150(2) | 150(2) |
| Crystal System | Monoclinic | Hexagonal | Hexagonal | Hexagonal | Hexagonal | Hexagonal |
| Space Group | *C*2/*c* (15) | $P6_322$ (182) | $P6_322$ (182) | $P6_322$ (182) | $P6_322$ (182) | $P6_322$ (182) |
| *a* (Å) | 11.2786(3) | 7.2350(3) | 7.2095(3) | 7.58190(10) | 7.5112(3) | 7.4866(7) |
| *b* (Å) | 9.1088(3) | 7.2350(3) | 7.2095(3) | 7.58190(10) | 7.5112(3) | 7.4866(7) |
| *c* (Å) | 7.0254(3) | 8.2926(4) | 8.1492(4) | 8.3786(2) | 8.0670(4) | 7.8898(8) |
| α (°) | 90 | 90 | 90 | 90 | 90 | 90 |
| β (°) | 96.6260(10) | 90 | 90 | 90 | 90 | 90 |
| γ (°) | 90 | 120 | 120 | 120 | 120 | 120 |
| V (Å$^3$) | 716.93(4) | 375.92(4) | 366.83(4) | 417.117(15) | 394.15(4) | 382.97(8) |
| Z | 4 | 2 | 2 | 2 | 2 | 2 |
| $\rho_{calc}$ (g cm$^{-3}$) | 2.552 | 2.469 | 2.528 | 2.571 | 2.754 | 2.833 |
| μ (cm$^{-1}$) | 8.565 | 8.694 | 11.807 | 5.865 | 6.709 | 7.197 |
| Refl. Meas./Unique | 7071/822 [$R_{int}$ = 0.043] | 3066/336 [$R_{int}$ = 0.029] | 2630/263 [$R_{int}$ = 0.026] | 9467/225 [$R_{int}$ = 0.046] | 3248/363 [$R_{int}$ = 0.028] | 3112/352 [$R_{int}$ = 0.048] |
| Parameters Refined | 55 | 19 | 19 | 21 | 19 | 19 |
| *R*1, *wR*2[a] (all) | 0.026, 0.053 | 0.017, 0.033 | 0.014, 0.032 | 0.020, 0.049 | 0.019, 0.038 | 0.030, 0.069 |
| *R*1, *wR*2[a] (obs) | 0.023, 0.053 | 0.015, 0.032 | 0.013, 0.032 | 0.019, 0.049 | 0.017, 0.037 | 0.027, 0.068 |
| $\chi^2$ | 1.09 | 1.12 | 1.18 | 1.36 | 1.163 | 1.09 |

[a] $w = 1/[\sigma^2(F_o^2) + (aP)^2 + bP]$ and $P = (\max(F_0^2, 0) + 2F_c^2)/3$; $R1 = \sum \left||F_o|-|F_c|\right| / \sum |F_o|$ and $wR2 = \sqrt{[(F_0^2 - F_c^2)^2 / \sum w(F_o^2)^2]}$

Phase purity of the samples created during this study were assessed using powder X-ray diffraction at ambient temperatures. This was carried out using a PANalytical Empyrean diffractometer, operating in Bragg-Brentano geometry, with monochromated Cu $K\alpha_1$ radiation and a PIXcel 1D detector. Diffraction patterns of $RbMn(HCO_2)_3$, $CsMn(HCO_2)_3$, $RbNi(HCO_2)_3$, and $RbCo(HCO_2)_3$, held on a glass plate, were fitted using the Le Bail method[28] in the program Rietica[29] and shown in Fig S1-4, confirming their purity. Diffraction patterns of $CsNi(HCO_2)_3$ and $CsCo(HCO_2)_3$ always indicated the presence of an impurity phase, which was unknown and whose structure it was not possible to identify.

Magnetic properties of samples determined to be pure phase by diffraction were characterized by Quantum Design magnetometers, either a MPMS 5 or MPMS XL instrument, equipped with 5 T superconducting magnets. Samples were enclosed in gelatin capsules mounted inside a pierced straw with a uniform diamagnetic background. Thermal stabilities were studied using a Perkin-Elmer TGA 7 Thermogravimetric Analyzer, with samples held in a platinum pan and heated at 10 °C min$^{-1}$. Infrared spectra were measured between 4000 cm$^{-1}$ and 500 cm$^{-1}$ using a Bruker Tensor-27 ATR spectrometer. These spectra have only four features present at about 2850 cm$^{-1}$ (C-H stretch), 1570 cm$^{-1}$ (C=O stretch), 1370 cm$^{-1}$ (C-O stretch) and 770-790 cm$^{-1}$ (O-C-O symmetric deformation).[30] The sharp O-C-O and C-O bands in $Rb(HCO_2)_3$ are split in two, indicating inclusion of two distinct formates.

## 3. Results and Discussion

### 3.1 Crystal Structures

Of the six compounds reported in this paper one of them, $RbMn(HCO_2)_3$, adopted the Perovskite II structure in *C*2/*c* monoclinic symmetry, with the remainder adopting $4^9{\bullet}6^6$ chiral hexagonal structures in $P6_322$ symmetry. The asymmetric unit of $RbMn(HCO_2)_3$ contains one $Rb^+$ cation, one $Mn^{2+}$ cation and one and a half formate anions, with the $Rb^+$, $Mn^{2+}$ and C atom on the second formate anion sitting on special positions with half the occupancy of the general position (see Fig. 2). The framework can be described as a heavily distorted $ReO_3$ structure with half the channels parallel to the *c*-axis occupied by $Rb^+$ cations, alternating along the *a*- and *b*-axis with channels occupied by hydrogen atoms from the ligand (see Fig. 3). The octahedral $Mn^{2+}$ are linked to six neighbouring octahedra through four equatorial *syn-anti* formate linkers and two axial *anti-anti* ligands along the *a*-axis, forming sheets of skewed squares. The presence of ligands with different coordination modes is consistent with splitting observed in the infrared spectra. The bond valence of the $Mn^{2+}$ cations are 2.08, consistent with a divalent cation.[31] The Mn-Mn intra-sheet distances are 5.7515(2) Å, significantly shorter

than the 6.290(3) Å inter-sheet distance, although the likely superexchange pathways for magnetic interactions are both about 6.85 Å. The $Rb^+$ cation is bonded to eight oxygen atoms with a bond valence of 1.21.[31] Down the directions in which octahedra are connected via formate bridges they can be viewed as being tilted out-of-phase with each other in a way resembling an $a^-a^-c^-$ Glazer tilt pattern.[32] The same tilt system is observed for the K-compounds[10,14] and the *C*2/*c* symmetry oxides with this tilt system is maintained despite the three atom formate bridge which skews the structure somewhat.

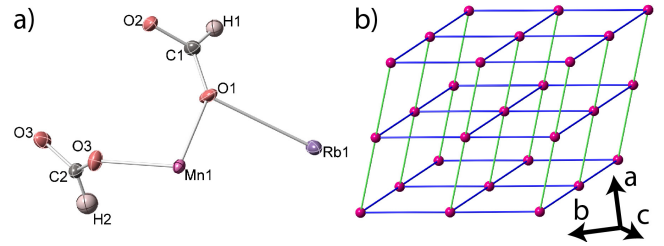


**Fig. 2:** a) The asymmetric unit of $RbMn(HCO_2)_3$ shown with 50 % probability ellipsoids. The $Mn^{2+}$, $Rb^+$, C, O and H atoms are pink, purple, black, red and pale pink. An additional oxygen atom, as required to complete the second formate ligand in the structure, is shown. b) The topology of the anionic $Mn(HCO_2)_3$ framework with axial and equatorial formate linkers shown in light green and dark blue.

The other five frameworks adopt the same chiral hexagonal structure reported for the $NH_4B(HCO_2)_3$ frameworks at room temperature (see Fig. 4 and 5 for depictions of $CsMn(HCO_2)_3$).[18] The asymmetric units of these compounds contain one alkali metal, one transition metal cation and half a formate ligand, most of the atoms in the structure are on special positions — the metals are on sites with a sixth of the occupancy of the general position and the H and C atoms on sites with half of the general occupancy. The octahedral transition metals in these materials have bond valencies of 2.06 for $CsMn(HCO_2)_3$ and between 1.96 and 1.98 for all remaining compounds, confirming divalent cations.[31] The chirality of this architecture comes from helical chains of these octahedra down the *c*-axis, linked by *syn-anti* formate linkers forming hexagonal channels; the A-site cations occupy these in highly distorted pseudo-octahedral sites, with bond valencies between 0.93-0.95.[31] The framework features puckered hexagonal sheets of transition metal cations linked by inter-sheet zigzag linkages, neighbouring transition metals in a sheet are significantly closer than between sheets (*c.f.* separations of 6.0589(1) Å to 8.3789(2) Å for $CsMn(HCO_2)_3$). This is consistent with the reported antiferromagnetic structures of the $NH_4B(HCO_2)_3$ compounds which reveals antiferromagnetic order of nearest neighbours in a sheet.[8] It was observed for $RbCo(HCO_2)_3$, $RbNi(HCO_2)_3$ and $CsMn(HCO_2)_3$ that the *a*-lattice parameter increases on heating while the *c*-lattice parameter shrinks, which is similar to the anisotropic negative thermal expansion in the $NH_4B(HCO_2)_3$ compounds and is likely due to a similar wine-rack mechanism.[8] As was also the case for $RbMn(HCO_2)_3$ a combination of single crystal and powder X-ray diffraction did not suggest any phase transitions occur in these materials between 150-300 K. This is not surprising as the phase transitions found in related structures are caused by hydrogen bonding between the molecular A-site cation and the framework, which alkali metals are unable to support.

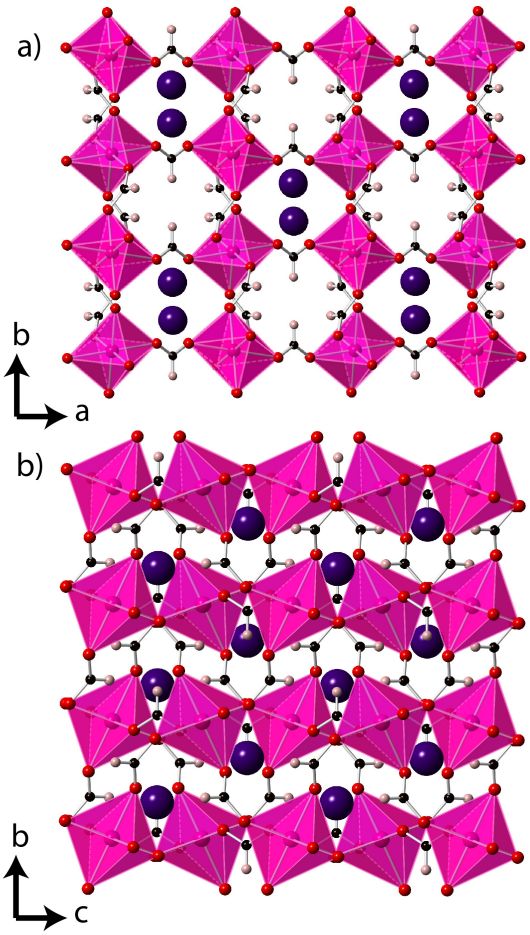


**Fig. 3**: The structure of $RbMn(HCO_2)_3$ showing a) the *ab* plane and b) the *bc* plane. The colours are the same as Fig 2.

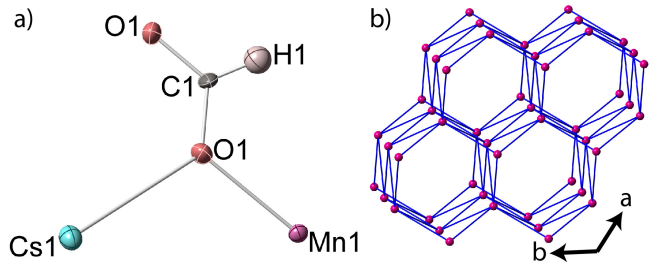


**Fig. 4:** a) The asymmetric unit of $CsMn(HCO_2)_3$ shown with 50 % probability ellipsoids. The $Cs^+$ atoms are represented in blue and all other colours are the same as Fig. 2. An additional $O^{2-}$, required to complete the formate in the structure, is shown. b) The topology of the anionic $Mn(HCO_2)_3$ framework with formate linkers shown in dark blue.

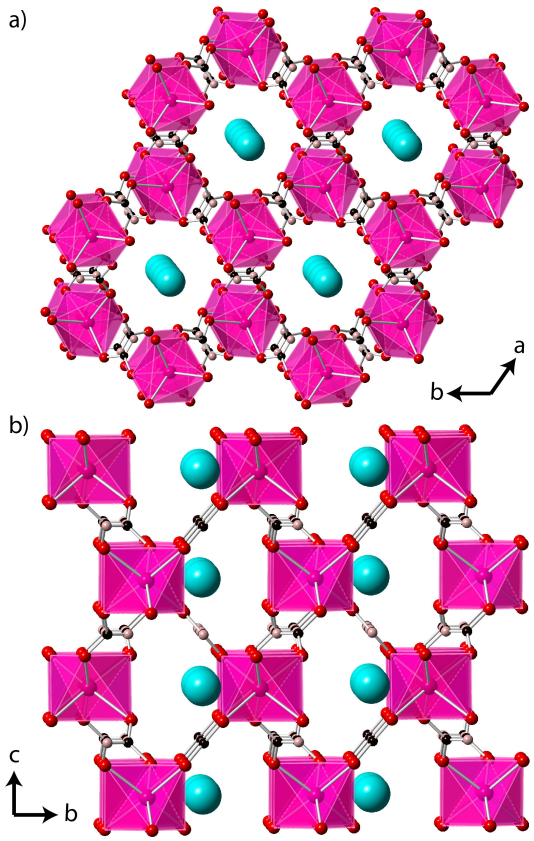


**Fig. 5:** The structure of $CsMn(HCO_2)_3$ showing a) the *ab* plane and b) the *bc* plane. The colours are the same as Fig. 4.

Tolerance factors for these six new phases were calculated using the method of Kielslich *et al*.[20] For $RbMn(HCO_2)_3$ $\alpha = 0.66$ and the other compounds have $0.68 < \alpha < 0.73$. This suggests that, when only monoatomic cations are present in an $AB(HCO_2)_3$ structure, the tolerance factor cut-off between the Perovskite II structure and the $4^9 \bullet 6^6$ chiral hexagonal phase is close to 0.66-0.68. This boundary is consistent with the observation of both phases for $KCo(HCO_2)_3$ whose $\alpha = 0.65$.[14] The Perovskite II structure of $KCo(HCO_2)_3$ is denser that the $4^9 \bullet 6^6$ chiral hexagonal phase,[14] which typically makes this structure more thermodynamically stable, as well established for other framework compounds.[33] If, however, the A-site cation is too large it appears that it becomes preferable for an $AB(HCO_2)_3$ framework to adopt the chiral hexagonal structure due to its larger channels (as a rough guide using a 1.1 Å probe in Mercury CSD 2.0[34] on the two $KCo(HCO_2)_3$ structures, from which $K^+$ has been removed, indicates that the channels in which the A-site cation sit take up 12.3 % and 2.5 % of the volume of the chiral hexagonal and Perovskite II phases, respectively). We checked for any indication of phase transformations in the new compounds reported in this work but did not notice any indication of this over a month.

This work clarifies the effect of ionic size on the evolution of the phases adopted by the larger $AB(HCO_2)_3$ family, with the $4^9 \bullet 6^6$ phase appearing to be formed for tolerance factors intermediate of the Perovskite I and Perovskite II phases (see Fig. 6). Based on our results we predict that the $KB(HCO_2)_3$ (B = $Fe^{2+}$, $Ni^{2+}$ and $Zn^{2+}$) frameworks, which have not been reported to date, would adopt the Perovskite II structure while $RbB(HCO_2)_3$ (B = $Fe^{2+}$ and $Zn^{2+}$) are likely to adopt the $4^9 \bullet 6^6$ phase. We propose that the tolerance factor range of the $4^9 \bullet 6^6$ phase is extended to lower values, for the $NH_4M(HCO_2)_3$ frameworks, and to higher values, for those including $HONH_3^+$ and $NH_2NH_3^+$ cations, because of the presence of hydrogen bonding between these molecular A-site cations and the framework, which the alkali metals cannot replicate.[5,18,19] This is likely because the directionality of hydrogen bonds means the number and strength of these bonds will depend on the precise shape of both the molecular cation and the architecture into which they are incorporated.

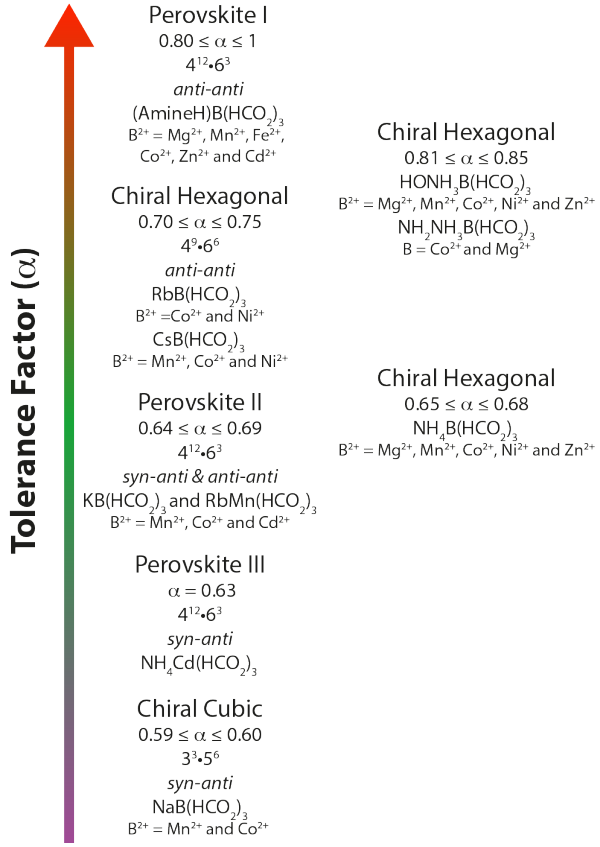


**Fig. 6:** The evolution of the structures of the known three dimensional $AB(HCO_2)_3$ frameworks with the tolerance factor, with an emphasis of the role of the molecular cations on the stability of the $4^9 \bullet 6^6$ at lower and higher tolerance factors than observed for monoatomic A-site cations.

### 3.2 Magnetic Properties

Magnetic property measurements were carried out on pure-phase, by diffraction, $RbB(HCO_2)_3$ and $CsMn(HCO_2)_3$ samples. The 100 Oe zero-field cooled (ZFC) susceptibility measurements of the $Rb^+$ containing phases exhibit a maximum in their magnetic susceptibility at 4, 9 and 27 K, for $Mn^{2+}$, $Co^{2+}$ and $Ni^{2+}$ (see Fig. 7 for $RbCo(HCO_2)_3$ and Fig. S5 and S6 for other $Rb^+$ frameworks); this is consistent with the onset of antiferromagnetic order. Below the ordering temperatures, however, the 100 Oe field cooled (FC) and ZFC measurements diverge indicating a ferromagnetic component is present. This

is suppressed rapidly with increasing applied fields so the ferromagnetic signal is essentially absent in fields over 1 kOe but clear, albeit subtle, hysteresis is observed in magnetization measurements of all three compounds, confirming the presence of a weak ferromagnetic component (see Fig. 8 for $RbCo(HCO_2)_3$ and Fig. S7 and S8 for other $Rb^+$ compounds). The magnetization measurements are not saturated at 50 kOe, consistent with predominantly antiferromagnetic behaviour.

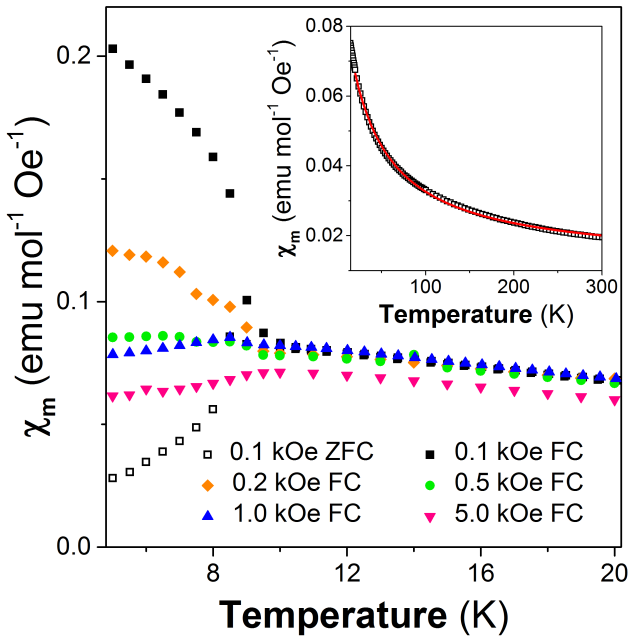


**Fig. 7:** Plot of variable temperature magnetic susceptibility measurements of $RbCo(HCO_2)_3$ in various magnetic fields with the insert showing the fit of the Curie-Weiss fit to the 100 Oe ZFC susceptibility measurement with a temperature independent component.

Weak ferromagnetic behaviour has previously been observed in the $(NH_4)B(HCO_2)_3$ and $KB(HCO_2)_3$ with similar ordering temperatures.[6,10,14,18] This was attributed to spin-canting, specifically due to Dzyaloshinsky-Moriya interactions in the $4^9 \bullet 6^6$ compounds, which lack an inversion centre,[6,18] and it is possible that symmetry lowering associated with magnetic ordering may also enable this in the Perovskite II structure. The magnetic susceptibility of $RbNi(HCO_2)_3$ increases further below 5 K, exhibiting a paramagnetic tail most likely caused by the presence of a trace impurity in the sample not detected by X-ray diffraction (see Fig S6). Above the Néel temperatures the behaviour of the Mn and Ni compounds are well fitted by Curie-Weiss behaviour with effective magnetic moments of 5.99 and 3.35 $\mu_B$, consistent with the expected values for octahedral $Mn^{2+}$ and $Ni^{2+}$, and Curie-Weiss temperatures of -6.0 K and -62 K (see Fig. S5 and S6). The magnetic susceptibility of $RbCo(HCO_2)_3$ could only be successfully fitted by the addition of an temperature independent term to the Curie-Weiss equation, yielding an effective magnetic moment of 4.61 $\mu_B$, a Curie-Weiss temperature of -29 K and a temperature independent term of $120 \times 10^{-4}$ emu $mol^{-1}$ $Oe^{-1}$ (see Fig. 7 insert). While the effective magnetic moment of $RbCo(HCO_2)_3$ is well within the range expected for octahedral $Co^{2+}$[35] it is somewhat lower than that reported for the isostructural $K^+$ and $NH_4^+$ phases, 5.5-5.6 $\mu_B$.[14,18]

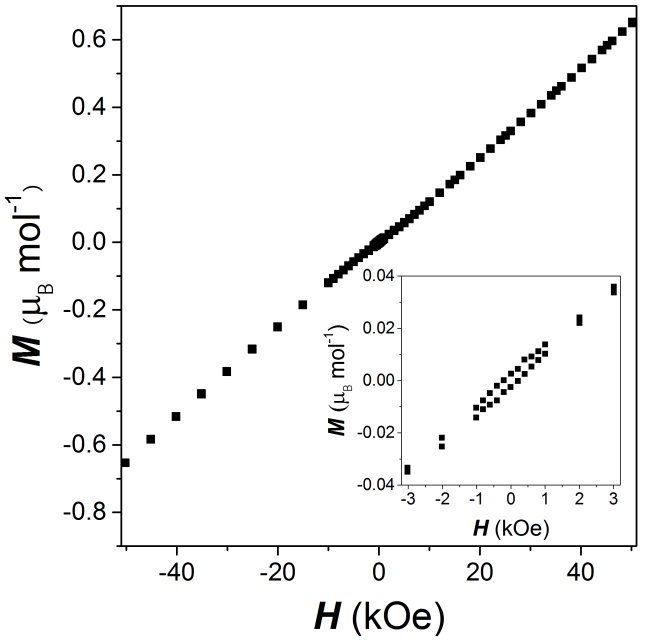


**Fig. 8:** Isothermal magnetisation measurements of $RbCo(HCO_2)_3$ at 5 K with the insert highlighting the subtle hysteresis at low applied magnetic fields.

The 100 Oe magnetic susceptibility measurements of $CsMn(HCO_2)_3$ reveal an antiferromagnetic cusp without deviation of the FC and ZFC measurements, consistent with purely antiferromagnetic behaviour below 9 K (see Fig. 9). Consistent with this a magnetization measurement at 5 K exhibits linear behaviour that does not saturate at the maximum field examined, 50 kOe. The magnetic susceptibility measurements in the paramagnetic phase can be well modelled by Curie-Weiss behaviour yielding a Curie-Weiss temperature of -13 K and an effective magnetic moment of 6.14 $\mu_B$, close to the expected spin-only value of 5.92 $\mu_B$ for high-spin $Mn^{2+}$ (see Fig. S9). The higher magnetic ordering temperature of this compound compared to the $RbMn(HCO_2)_3$ phase indicates that the magnetic interactions in the chiral hexagonal phases are significantly stronger than in the Perovskite II phase. This is consistent with a comparison of the other known compounds with these structures, which shows that interchanging between the $NH_4^+$, $K^+$, $Rb^+$ and $Cs^+$ cations does not significantly change the magnetic ordering temperature provided the structure and the transition metal remains the same; changing from the chiral hexagonal structure to the Perovskite II structure, however, systematically weakens the magnetic interactions in these materials regardless of the transition metal present.[6,10,14,18] This emphasises the importance of understanding the structure-property relationship in the complex $AB(HCO_2)_3$ family of compounds in the search for new functional magnetic materials.

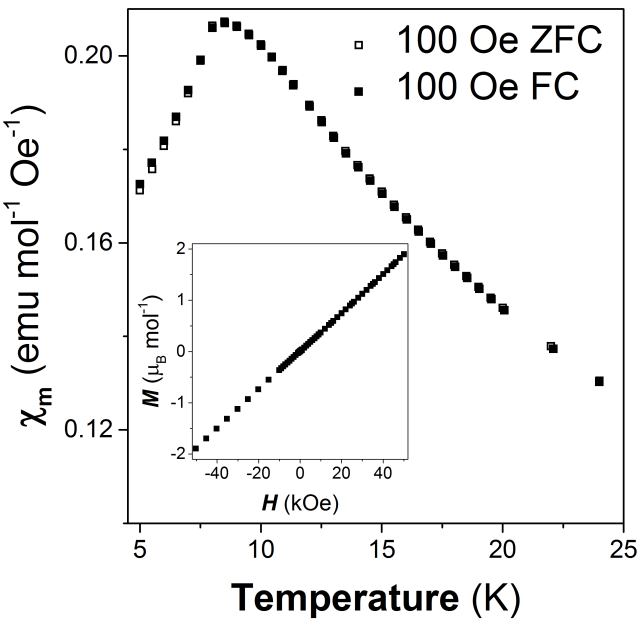


**Fig. 9:** Plot of variable temperature magnetic susceptibility measurements of $CsMn(HCO_2)_3$ in a 100 Oe applied field with an insert displaying its isothermal magnetisation measured at 5 K.

### 3.3 Thermal Stability

Thermogravimetric analysis carried out in air suggest that $RbMn(HCO_2)_3$, $RbCo(HCO_2)_3$, $RbNi(HCO_2)_3$ and $CsMn(HCO_2)_3$ begin to decompose at approximately 180, 210, 200 and 190 °C and is essentially complete by between 400 and 450 °C (see Fig S10-13). The bulk of the weight loss occurs in one step, as observed for other alkali metal formates, with weights at the end of this step consistent with the formation of alkali metal carbonates and metal oxides.[10,14,17] Only the decomposition of $RbMn(HCO_2)_3$ is delayed significantly when carried out in nitrogen, occurring at 270 °C, while all other compounds examined begin to decompose within 20 °C of the temperature at which they do in air. Duan *et al.*[14] have previously suggested that the decomposition pathway of $KCo(HCO_2)_3$ is different depending on whether it adopts the Perovskite II or chiral hexagonal polymorph and it is also possible that the differences in the structures of these materials may have some effect on their decomposition pathways in the absence of oxygen. The decomposition temperatures observed for these $Rb^+$ and $Cs^+$ compounds is somewhat lower than those observed for $AB(HCO_2)_3$ frameworks containing $Na^+$ or $K^+$, which are reported to decompose above 330 and 230 °C, respectively.[10,14,17] This suggests that the thermal stability of this family of alkali frameworks decreases significantly with increasing size of the A-site cation, likely because their decreased charge density leads to weaker interactions between them and the anionic framework.

## 4. Conclusions

This study reports the structure of six new $AB(HCO_2)_3$ frameworks, where A = $Rb^+$ or $Cs^+$ and B = $Mn^{2+}$, $Co^{2+}$ or $Ni^{2+}$. $RbMn(HCO_2)_3$ adopts a perovskite-like structure with $4^{12}\bullet6^3$ topology with a mixture of *syn-anti* and *anti-anti* ligand coordination modes, while the other five compounds in this study all exhibit a chiral hexagonal structure with $4^9\bullet6^6$ topology. Adding this knowledge to the structure of known related compounds we have proposed a phase diagram rationalising the effect of ionic size on the formation of the various structures known to be formed by the $AB(HCO_2)_3$ frameworks, in particular clarifying the placement of the $4^9\bullet6^6$ chiral hexagonal frameworks within this. This also emphasises the likely importance of hydrogen bonding in stabilising the chiral hexagonal phases, which are commonly reported to be ferroelectric, compared to perovskite-like topologies where a molecular A-site cation is present. The $Rb^+$ containing compounds were all found to be weak ferromagnets, most likely due to spin canting, while $CsMn(HCO_2)_3$ appears to be an antiferromagnet. The magnetic interactions in $RbMn(HCO_2)_3$ are much weaker than in the other compounds reported in this study, confirming the trend that the magnetic interactions in the perovskite-like structure it adopts are much weaker than in the $4^9\bullet6^6$ phases.

## Acknowledgements

We would like to thank Amber Thompson for help with single crystal X-ray diffraction. The authors would like to thank the Glasstone Trust for funding via the provision of a fellowship.

## Notes and references

i We have (re)calculated the tolerance factors throughout this manuscript using the ionic radii of the high spin state, as determined by Shannon,[36] found experimentally to be adopted by the paramagnetic B-site cations in these compounds. For consistency with Gómez-Aguirre et al.,[11] we have used the relevant eight coordinate ionic radii for the alkali metals.[36]

1. a) C. N. R. Rao, A. K. Cheetham and A. Thirumurugan, *J. Phys.: Condens. Matter*, 2008, **20**, 083202; b) M. Kurmoo, *Chem. Soc. Rev.*, 2009, **38**, 1353-1379; c) G. Givaja, P. Amo-Ochoa, C. J. Gomez-Garcia and F. Zamora, *Chem. Soc. Rev.*, 2012, **41**, 115-147; d) P. J. Saines, M. Steinmann, J.-C. Tan, W. Li, P. T. Barton and A. K. Cheetham, *Inorg. Chem.*, 2012, **51**, 11198-11209; e) G. Lorusso, J. W. Sharples, E. Palacios, O. Roubeau, E. K. Brechin, R. Sessoli, A. Rossin, F. Tuna, E. J. L. McInnes, D. Collison and M. Evangelisti, *Adv. Mater.*, 2013, **25**, 4653-4656; f) P. Ramaswamy, N. E. Wong and G. K. H. Shimizu, *Chem. Soc. Rev.*, 2014, **43**, 5913-5932; g) P. J. Saines, P. T. Barton, M. Jura, K. S. Knight and A. K. Cheetham, *Mater. Horiz.*, 2014, **1**, 332-337; h) F.-S. Ke, Y.-S. Wu and H. Deng, *J. Solid State Chem.*, 2015, **223**, 109-121.
2. M. Kurmoo, H. Kumagai, K. W. Chapman and C. J. Kepert, *Chem. Commun.*, 2005, 3012-3014.
3. G. Rogez, N. Viart and M. Drillon, *Angew. Chem. Int. Ed.*, 2010, **49**, 1921-1923.
4. Z. Wang, K. Hu, S. Gao and H. Kobayashi, *Adv. Mater.*, 2010, **22**, 1526-1533.

5. S. Chen, R. Shang, K.-L. Hu, Z.-M. Wang and S. Gao, *Inorg. Chem. Fron.*, 2014, **1**, 83-98.
6. G.-C. Xu, W. Zhang, X.-M. Ma, Y.-H. Chen, L. Zhang, H.-L. Cai, Z.-M. Wang, R.-G. Xiong and S. Gao, *J. Am. Chem. Soc.*, 2011, **133**, 14948-14951.
7. G. J. Halder, C. J. Kepert, B. Moubaraki, K. S. Murray and J. D. Cashion, *Science*, 2002, **298**, 1762-1765.
8. J. M. M. Lawler, P. Manuel, A. L. Thompson and P. J. Saines, *Dalton Trans.*, 2015, **44** 11613-11620.
9. B. Pato-Doldan, L. C. Gomez-Aguirre, J. M. Bermudez-Garcia, M. Sanchez-Andujar, A. Fondado, J. Mira, S. Castro-Garcia and M. A. Senaris-Rodriguez, *RSC Adv.*, 2013, **3**, 22404-22411.
10. E. Eikeland, N. Lock, M. Filsø, M. Stingaciu, Y. Shen, J. Overgaard and B. B. Iversen, *Inorg. Chem.*, 2014, **53**, 10178-10188.
11. L. C. Gómez-Aguirre, B. Pato-Doldán, A. Stroppa, S. Yáñez-Vilar, L. Bayarjargal, B. Winkler, S. Castro-García, J. Mira, M. Sánchez-Andújar and M. A. Señarís-Rodríguez, *Inorg. Chem.*, 2015, **54**, 2109-2116.
12. P. Jain, V. Ramachandran, R. J. Clark, H. D. Zhou, B. H. Toby, N. S. Dalal, H. W. Kroto and A. K. Cheetham, *J. Am. Chem. Soc.*, 2009, **131**, 13625-13627.
13. G. Kieslich, S. Sun and A. K. Cheetham, *Chem. Sci.*, 2015, **6**, 3430-3433.
14. Z. Duan, Z. Wang and S. Gao, *Dalton Trans.*, 2011, **40**, 4465-4473.
15. A. Antsyshkina, M. A. Porai-Koshits, V. N. Ostrikova and G. G. Sadikov, *Sov. J. Coord. Chem.*, 1983, **9**, 855-858.
16. V. Paredes-García, A. Vega, M. A. Novak, M. G. F. Vaz, D. A. Souza, D. Venegas-Yazigi and E. Spodine, *Inorg. Chem.*, 2009, **48**, 4737-4742.
17. J.-P. Zhao, S.-D. Han, R. Zhao, Q. Yang, Z. Chang and X.-H. Bu, *Inorg. Chem.*, 2013, **52**, 2862-2869.
18. Z. Wang, B. Zhang, K. Inoue, H. Fujiwara, T. Otsuka, H. Kobayashi and M. Kurmoo, *Inorg. Chem.*, 2007, **46**, 437-445.
19. B. Liu, R. Shang, K.-L. Hu, Z.-M. Wang and S. Gao, *Inorg. Chem.*, 2012, **51**, 13363-13372.
20. G. Kieslich, S. Sun and A. K. Cheetham, *Chem. Sci.*, 2014, **5**, 4712-4715.
21. L. Chen, H. Jin, J. Wang, Y. Zhou, W. Zhu and Q. Zhou, *Cryogenics*, 2013, **54**, 54-58.
22. Z. Otwinowski and W. Minor, in *Methods Enzymol.*, ed. Charles W. Carter, Jr., Academic Press, 1997, vol. 276, pp. 307-326.
23. *CrysAlis PRO* 171.36.32, Agilent Technologies, Yarnton, Oxfordshire, England, 2014.
24. G. Sheldrick, *Acta Crystallogr.*, 2008, **A64**, 112-122.
25. G. Oszlanyi and A. Suto, *Acta Crystallogr.*, 2008, **A64**, 123-134.
26. G. Sheldrick, *Acta Crystallogr.*, 2015, **C71**, 3-8.
27. O. V. Dolomanov, L. J. Bourhis, R. J. Gildea, J. A. K. Howard and H. Puschmann, *J. Appl. Crystallogr.*, 2009, **42**, 339-341.
28. A. Le Bail, H. Duroy and J. L. Fourquet, *Mater. Res. Bull.*, 1988, **23**, 447-452.
29. B. A. Hunter and C. J. Howard, *A computer program for Rietveld analysis of X-ray and neutron powder diffraction patterns,*, Lucas Heights Laboratories, 1998.
30. K. Nakamoto, *Infrared and Raman Spectra of Inorganic and Coordination Compounds*, John Wiley & Sons, Inc., 2008.
31. N. E. Brese and M. O'Keeffe, *Acta Crystallogr.*, 1991, **B47**, 192-197.
32. C. J. Howard and H. T. Stokes, *Acta Crystallogr.*, 1998, **B54**, 782-789.
33. a) K. C. Kam, K. L. M. Young and A. K. Cheetham, *Cryst. Growth Des.*, 2007, **7**, 1522-1532; b) H. H. M. Yeung, M. Kosa, M. Parrinello and A. K. Cheetham, *Cryst. Growth Des.*, 2013, **13**, 3705-3715.
34. C. F. Macrae, I. J. Bruno, J. A. Chisholm, P. R. Edgington, P. McCabe, E. Pidcock, L. Rodriguez-Monge, R. Taylor, J. van de Streek and P. A. Wood, *J. Appl. Crystallogr.*, 2008, **41**, 466-470.
35. A. R. West, *Solid State Chemistry and Its Applications*, John Wiley & Sons Inc., Second Edn., 2014.
36. R. Shannon, *Acta Crystallogr.*, 1976, **A32**, 751-767.